

## RESEARCH

# IR-UWB Detection and Fusion Strategies using Multiple Detector Types

Vijaya Yajnanarayana, Satyam Dwivedi and Peter Händel

Full list of author information is available at the end of the article

## Abstract

Optimal detection of ultra wideband (UWB) pulses in a UWB transceiver employing multiple detector types is proposed and analyzed in this paper. To enable the transceiver to be used for multiple applications, the designers have different types of detectors such as energy detector, amplitude detector, etc., built in to a single transceiver architecture. We propose several fusion techniques for fusing decisions made by individual IR-UWB detectors. In order to get early insight into theoretical achievable performance of these fusion techniques, we assess the performance of these fusion techniques for commonly used detector types like matched filter, energy detector and amplitude detector under Gaussian assumption. These are valid for ultra short distance communication and in UWB systems operating in millimeter wave (mmwave) band with high directivity gain. In this paper, we derive the detection performance equation for each of the detectors in terms of false alarm rate, shape of the pulse, and number of UWB pulses used in the detection and apply these in the fusion algorithms. We show that the performance can be improved approximately by 4 dB in terms of signal to noise ratio (SNR) for high probability of detection of a UWB signal ( $> 95\%$ ), by fusing decisions from multiple detector types compared to standalone energy detector, in a practical scenario.

**Keywords:** Neyman-Pearson test; Sensor Networks; Time of Arrival (TOA); Ultra Wideband (UWB); UWB ranging

## 1 Introduction

An ultra wideband (UWB) communication system is based on spreading a low power signal into wideband. There are several techniques to spread a low power signal to wideband including OFDM (orthogonal frequency division multiplexing), DSS (direct spread spectrum), FH (frequency hopping), and IR (impulse radio). Impulse radio based UWB (IR-UWB) schemes are most popular as they provide better performance and complexity trade-offs compared to other UWB schemes [1–3].

IR-UWB schemes employ narrow impulse signals, which can yield high time resolution, and hence can be used for accurate position localization and ranging. Narrow pulse duration coupled with low amplitude due to the restriction from regulatory agencies like Federal Communications Commission (FCC) makes the detection of these pulses challenging [4–6]. Generally, transmit signaling employs multiple pulses and the receiver aggregates certain characteristics from these pulses like energy, amplitude, position, etc., to make statistical inferences on the transmitted information like range (localization) or transmitted symbol value (communication) etc. [2, 7]. The performance of the receiver depends on how well the received pulse statistics are utilized for a chosen application [6, 8].

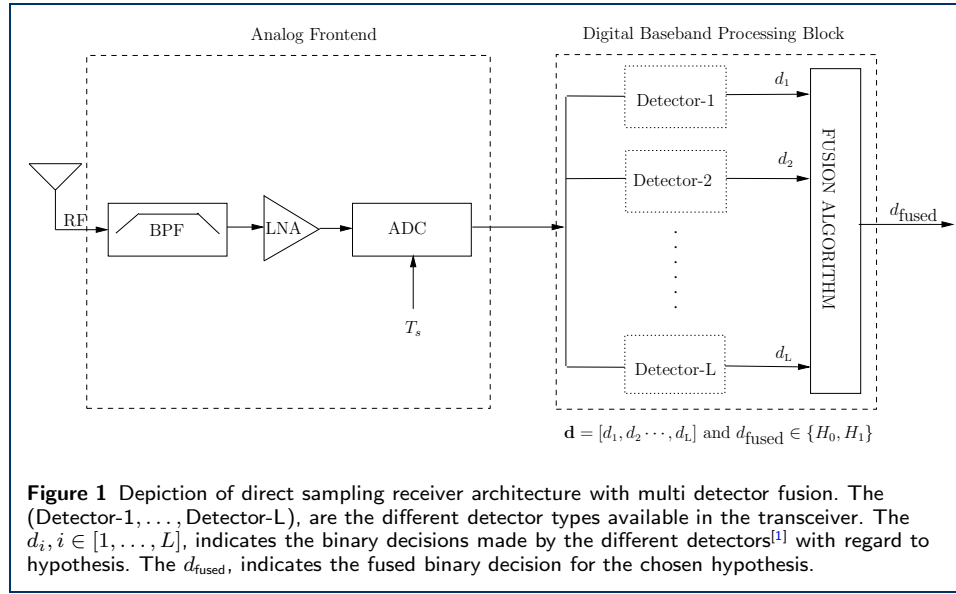
In this paper, we will consider the structure of a digital sampling receiver shown in Fig. 1. The received signal is filtered by an RF band-pass filter (BPF) and is amplified using a wideband LNA. The signal is then converted into the digital domain by a high sampling rate ADC and digitally processed. The digital receiver structure offers several benefits such as flexibility in design, reconfigurability and scalability [9]. However, since IR-UWB signals occupy large bandwidth and have high time resolution, the design of an IR-UWB digital transceiver is challenging. In order to exploit the regulatory body specifications optimally, the transceivers must operate at a 3.1 – 10 GHz range or in the unlicensed millimeter wave (mmwave) frequency. The wideband BPF design should cover the whole of the useful UWB frequency band. The microwave filter's design, based on microstrip multi-mode resonator (MMR) and hybrid coplanar waveguide/microstrip structure can cover these ranges. The work in [10–13] proposes several wideband BPF filter designs for the intended purpose. The wideband LNA amplifies the signal to the operating levels of the analog to digital converters (ADC). The work in [14, 15] discusses the various design aspects of the wideband LNA for UWB radios.

The most complex and costly part of the IR-UWB digital receiver is the ADC. IR-UWB pulses are extremely narrow (order of few ns) and occupy very high bandwidth, therefore high speed ADCs are needed for faithful digital representation of the IR-UWB pulses. Typically, such high speed ADC are designed using flash ADC [16] or a bank of polyphase ADCs [17]. The recent progress in the ADC technology, as suggested by [18], indicates that such high speed ADC having good resolution with signal to noise and distortion ratio (SNDR) of higher than 30 dB can be achieved for a bandwidth of 10 GHz. This has enabled the digital designs for IR-UWB technology.

The digital samples from the ADC will be processed by a digital baseband processing block for detection. In many hardware platforms, a single UWB transceiver mounted on sensors is used for multiple applications like ranging, localization, communication, etc., each using particular statistics of the received samples for UWB pulse detection [19]. For example, large distance communication using UWB may employ energy detector over a large number of pulses; whereas short distance tracking application may use amplitude detector on a few pulses. To enable the transceiver to be used for multiple applications, the designers have different types of detectors like amplitude detector, energy detector, etc., built into a single transceiver. Each detector<sup>[1]</sup> uses its own detection algorithm on the received samples to infer a hypothesis from the received samples and report it to the higher layers for further processing. These are typically implemented in FPGA for faster processing, and hence, only the computed hard or soft-value decisions are available. In some applications, there are no stringent constraints to bind the usage of a particular detector type; for example, demodulation of short range low rate communication data. In these situations, instead of resorting to a single detector type to arrive at the hypothesis, decision information from all of the different types of detectors can be concurrently utilized to make more informed decision on the hypothesis. This will utilize transceiver infrastructure better, and since every detector

---

<sup>[1]</sup>Detectors and detector types are interchangeably used. In Fig. 1, each detector in the set, (Detector-1, ..., Detector-L) are of different type.



decision is new information about the signaled hypothesis, it should yield better reliability and improved performance.

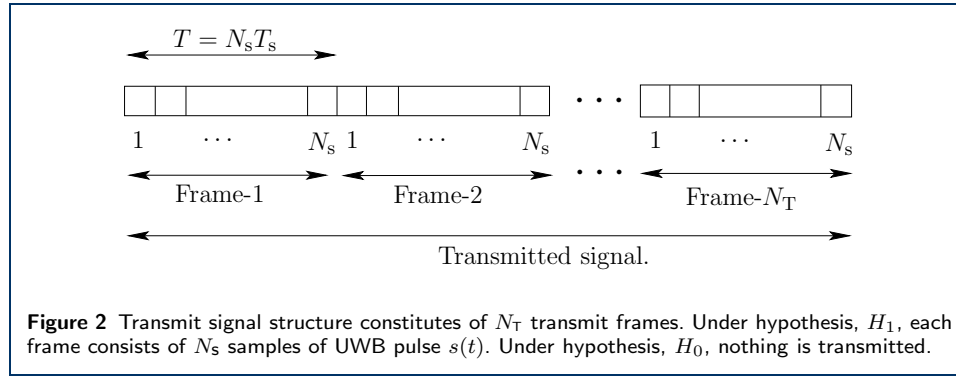
The proposed transceiver structure shown in Fig. 1, is applicable to the future evolution of our in-house flexible UWB hardware platform [20, 21]. This platform can be used for joint ranging and communication applications. The platform has a digital processing section comprising of an FPGA, where the proposed techniques of this paper can be implemented. Even though the applicability of the techniques are demonstrated in simulation, the results provide an early insight in to achievable performance. The variant of the proposed structure in Fig. 1 for hypotheses testing are also employed in [22] and [23]. In [22], the authors discuss the UWB hypothesis testing for a bank of similar analog detectors, where as in [23], authors proposes a distributed fusion of results from multiple UWB sensors, by allocating the different number of pulses to each sensor, under the constraint of maximum number of allocated pulses, such that the error is minimized. Thus, both are different from the proposed application of this paper.

In this paper, we formulate a binary hypothesis problem of IR-UWB pulse detection, where decisions from different types of detectors are fused using different fusion methods before deciding on the hypothesis as shown in Fig. 1. We demonstrate the methods using three commonly employed UWB detector-types ( $L = 3$  in Fig. 1), having energy detector (ED), matched filter (MF), and amplitude detector (AD) for Detector-1, Detector-2 and Detector-3 respectively. The binary decisions signaling the hypothesis from these three detectors  $\mathbf{d} = [d_1, d_2, d_3]$  are fed to the fusion algorithm to arrive at the binary decision regarding the hypothesis,  $d_{fused}$ .

To illustrate the benefits of the scheme, we perform the following steps. First, we discuss the fusion algorithms for a set of different detectors types (Detector-1, ..., Detector-L), yielding binary decisions signaling the hypothesis,  $\mathbf{d}$ , (refer to Fig. 1). Subsequently, we derive performance equations for the most commonly used IR-UWB detector types like matched filter (MF), amplitude detector (AD) and energy detector (ED). Here, we derive analytical expression for proba-

**Table 1** Parameters on which detectors performance depends.

Parameter	Description
$P_{FA}$	Probability of false alarm
SNR	Signal to noise ratio
$N_p$	Number of UWB pulses used in detection
$E_p$	Energy of the UWB pulses
$s(t)$	Shape of the UWB pulses



bility of detection,  $P_D$ , as a function of false alarm rate,  $P_{FA}$ , and signal-to-noise ratio, SNR, for a multi-pulse UWB signal corrupted by additive white Gaussian noise (AWGN). Then, we use these expressions in the fusion algorithms discussed earlier with  $L = 3$  and Detector-1, Detector-2 and Detector-3 as MF, ED and AD respectively to assess the performance.

The rest of the paper is organized as follows. In Section 2, we will discuss the system model. Here, we will define the signal model which will be used in the rest of the paper. Section 3, discusses different fusion strategies. In Section 4, we will derive analytical expression for  $P_D$  as a function of  $P_{FA}$ , and SNR for matched filter, energy detector and amplitude detector for multi-pulse IR-UWB signal. In Section 5, we will evaluate the performance of the different fusion strategies using the performance equation of the individual detectors derived in Section 4. Finally in Section 6, we discuss the conclusions.

## 2 System Model

We consider a binary hypothesis for detection, with  $H_0$  representing signal is absent and  $H_1$  representing signal is present. Each of the different types of detectors like MF, ED, etc., in the UWB transceiver constructs a test statistic from the received samples, based on which inference is made about  $H_0$  or  $H_1$  by comparing the test statistic to some threshold,  $\gamma$ . Different detector types have different ways to construct the test statistic, and thus have varying degrees of performance like probability of detection,  $P_D$ , probability of error,  $P_e$ , etc. Apart from the chosen test statistic, the performance of the particular detector also depends on all or few of the parameters listed in the Table 1. In Section 4, we will derive analytical expression for probability of detection,  $P_D$ , for the ED, MF, and AD detectors as a function of parameters defined in Table 1.

The transmitted signal under hypothesis  $H_1$  consists of  $N_T$  frames, such that

$$N_T \geq N_p^i \quad \forall i \in [1, 2, \dots, L],$$

where,  $N_p^i$ , denotes the number of frames used by Detector- $i$  in the hypothesis test. Each frame consists of one IR-UWB pulse, and during hypothesis  $H_0$  nothing is transmitted ( $N_T$  empty frames). Each UWB pulse is of fixed duration,  $T$ , represented by  $s(t)$ , sampled at the rate,  $1/T_s$ , and has  $N_s = T/T_s$ , samples. The transmit signal structure is as shown in Fig. 2. Thus, both hypotheses can be mathematically expressed as

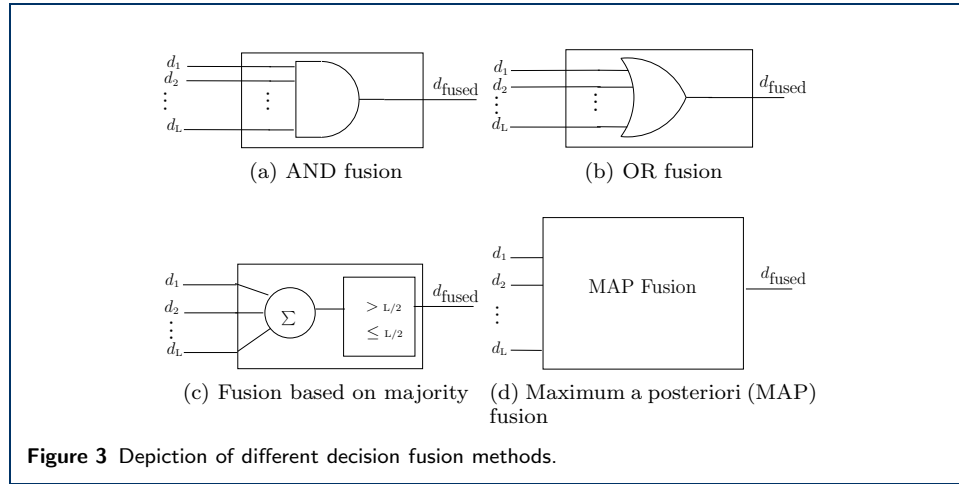
$$\begin{aligned} & \sum_{n=0}^{N_T-1} \sum_{i=0}^{N_s-1} s(t-nT)\delta(t-nT-iT_s) \quad \text{under } H_1 \\ & 0 \quad \text{under } H_0 \end{aligned}, \quad (1)$$

where,  $\delta(t)$ , denotes the Dirac delta function and the model uses  $N_T$  identical frames in each hypothesis test cycle. This is similar to time hopped impulse radio (TH-IR) UWB models proposed in [1,2,24], except that we are not considering time hopping, as it has no effect on the statistics collected by the detector across multiple frames. The function,  $s(t-nT)\delta(t-nT-iT_s)$ , represents  $i$ -th discrete sample of the  $n$ -th frame under hypothesis  $H_1$  and is denoted by  $s(n,i)$ . The received signal is corrupted by Gaussian noise. Thus, the received signal used in the hypothesis test under both hypotheses is given by

$$\begin{aligned} & \sum_{n=0}^{N_T-1} \sum_{i=0}^{N_s-1} x(t-nT)\delta(t-nT-iT_s) \quad \text{under } H_1 \\ & \sum_{n=0}^{N_T-1} \sum_{i=0}^{N_s-1} w(t-nT)\delta(t-nT-iT_s) \quad \text{under } H_0 \end{aligned}, \quad (2)$$

where,  $x(t)$ , is the received pulse shape. The function,  $x(t-nT)\delta(t-nT-iT_s)$ , represents the  $i$ -th sample of the  $n$ -th received frame under hypothesis  $H_1$  and is denoted by  $x(n,i)$ . Similarly,  $w(t-nT)\delta(t-nT-iT_s)$ , represents the Gaussian noise corresponding to the  $i$ -th sample of the  $n$ -th received frame and is denoted by  $w(n,i)$ . We assume a single-path line of sight (LOS) channel, thus, the received samples,  $x(n,i) = \beta s(n,i) + w(n,i)$ , where,  $\beta$ , indicates the path loss.

Typically, the UWB channels are subject to multi-path propagation, where a large number of paths can be observed at the receiver. However, if the transceivers are in close proximity with clear line of sight, the detectors here rely on the first arriving path or LOS, this is in contrast to traditional channel measurement and modeling. If the UWB transceiver is operating at millimeter wave frequencies, due to the combined effect of higher directivity gain due to the RF-beamforming and higher absorption characteristics of the channel results in single-path LOS channels for distances less than 100 meters. The IEEE 802.15.3c standard channel measurements for residential LOS channel model (CM1), also corroborate the same [25–27]. For the transceiver operating in the frequency band less than 10 GHz, due to higher reflections, refractions and scattering characteristics of the channel, the assumptions of single-path LOS channel is valid only for extremely short distance of order less than 10 meters [20, 21, 28, 29]. These short distance high speed UWB applications include transferjet and wireless USB (wUSB) [30, 31]. Also, adopting a simple model proposed here will make the discussion mathematically tractable. Without loss of generality, we use  $\beta = 1$ .



In the next Section, we will discuss the fusion strategies for fusing individual detector decisions (refer to Fig. 1).

### 3 Fusion Rules for IR-UWB Signal Detection

One way to fuse the detector output shown in Fig 1, is to use  $k$  out of  $L$  decision approach, where the fused decision will be hypothesis  $H_1$ , if at least  $k$  out of  $L$  detectors decide on hypothesis  $H_1$ . If we define the decision of the  $i$ -th detector in the Fig. 1, as  $d_i = 1$  and  $d_i = 0$ , for hypotheses  $H_1$  and  $H_0$  respectively, special cases of  $k$  out of  $L$ , fusion rules can be implemented by fusing individual detector decisions, ( $d_i$ 's), using logical functions like “AND”, “OR” and “Majority decision”. These types of fusion methods are studied in [32–35]. Here, we try to assess their performance in the IR-UWB pulse detection problems discussed earlier. The fusion rule for “AND”, “OR”, and “majority decision”, will have  $k = L$ ,  $k = 1$  and  $k > L/2$ , respectively; where  $L$  is the number of detector decisions used in the fusion. These fusion rules are depicted in the Fig. 3a, Fig. 3b and Fig. 3c.

The  $k$  out of  $L$  detection is biased either toward hypothesis  $H_1$  (UWB pulse detection in our model), or toward  $H_0$ . For example, fusing using the “OR” rule will have superior detection performance, but will also have a larger false alarm rate. Similarly, the “AND” fusion rule is conservative in UWB pulse detection, but has superior false alarm rate performance. These aspects are further illustrated with numerical examples in the later sections. If we define the mis-classification of the hypothesis as an error and the objective is to minimize the probability of error,  $P_e$ , then the decision rule discussed above are sub-optimal. This is motivation to design a fusion technique that is optimal in probability of error sense. For any prior probability for  $H_0$  and  $H_1$ , the fusion rule that minimizes the probability of error is given by maximum a posteriori (MAP) formulation given below.

$$\Pr(H_1|\mathbf{d}) \underset{H_0}{\overset{H_1}{\gtrless}} \Pr(H_0|\mathbf{d}). \quad (3)$$

Where,  $\mathbf{d}$ , is a  $L$ -size vector of binary values signaling the hypothesis of the decisions made by different detectors (refer to Fig. 1). We can write (3) as

$$\log \left( \frac{\Pr(H_1|\mathbf{d})}{\Pr(H_0|\mathbf{d})} \right) \underset{H_0}{\overset{H_1}{\geq}} 0. \quad (4)$$

If we define sets  $\mathcal{I}$ ,  $\mathcal{S}_{H_1}$  and  $\mathcal{S}_{H_0}$  as

$$\mathcal{I} := \{1, 2, \dots, L\}, \quad (5)$$

$$\mathcal{S}_{H_1} := \{i : d_i = 1\}, \quad (6)$$

$$\mathcal{S}_{H_0} := \mathcal{I} \setminus \mathcal{S}_{H_1} := \{i : d_i = 0\}, \quad (7)$$

where,  $d_i$ , is the binary decision of the detector- $i$  ( $i \in \mathcal{I}$ ), then,

$$\Pr(H_1|\mathbf{d}) = \frac{P_1}{p(\mathbf{d})} \prod_{i \in \mathcal{S}_{H_1}} P_D^i \prod_{i \in \mathcal{S}_{H_0}} (1 - P_D^i) \quad (8)$$

Here, we assumed that the decisions of each of the detectors are independent of each other.  $P_1$  is the probability of hypothesis  $H_1$  and  $p(\cdot)$  denote the probability density function (PDF).  $P_D^i$  is the probability of detection of the detector- $i$  in Fig. 1. Similarly, we can write

$$\Pr(H_0|\mathbf{d}) = \frac{P_0}{p(\mathbf{d})} \prod_{i \in \mathcal{S}_{H_1}} P_{FA}^i \prod_{i \in \mathcal{S}_{H_0}} (1 - P_{FA}^i) \quad (9)$$

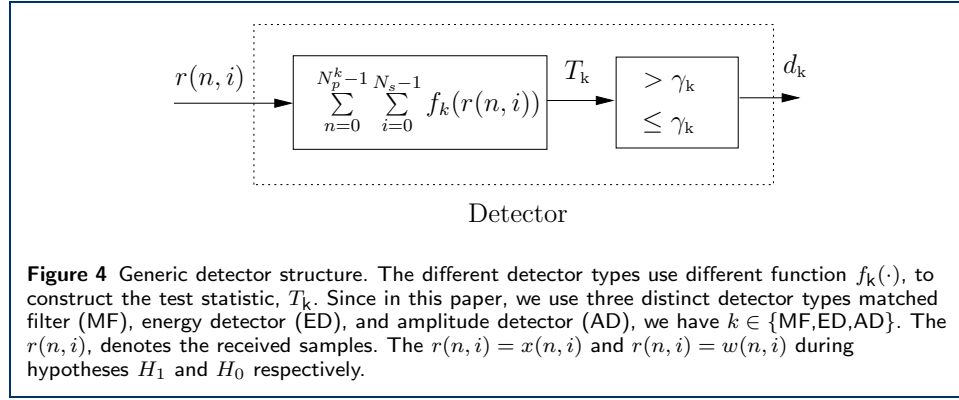
$P_0$  is the probability of hypothesis  $H_0$ .  $P_{FA}^i$  is the false alarm of the  $i$ -th detector. In many applications such as in communication, hypothesis testing is used for symbol decoding, where both the hypotheses are equally likely. Substituting (8) and (9) in (4) and assuming both hypotheses are equally likely, we get the decision rule as

$$\log \left( \frac{\Pr(H_1|\mathbf{d})}{\Pr(H_0|\mathbf{d})} \right) = \sum_{i \in \mathcal{S}_{H_1}} \log \left( \frac{P_D^i}{P_{FA}^i} \right) + \sum_{i \in \mathcal{S}_{H_0}} \log \left( \frac{(1 - P_D^i)}{(1 - P_{FA}^i)} \right) \underset{H_0}{\overset{H_1}{\geq}} 0. \quad (10)$$

In order to assess the performance of these fusion rules, the detection performance ( $P_D^i$  and  $P_{FA}^i$ ) of the individual detector should be known. The most common types of IR-UWB detectors include matched filter, energy detector and amplitude detector. In the next Section, we will derive the detection performance of these detectors, which will be used in the later Sections to evaluate the fusion performance.

## 4 Detector Performance

The performance of the MF, ED, and AD detectors are studied in [36–39] for a general deterministic signals. Energy detection based sub-Nyquist UWB detectors are studied in [40, 41]. However, the performance analysis of the MF, ED, and AD detection for a digital UWB signal as a function of parameters shown in Table 1, is not available in literature to the best knowledge of the authors. In this Section, we will derive analytical expressions for probability of detection,  $P_D$ , as a function of



parameters in Table 1 and use them in later Sections to assess the performance of the fusion rules discussed in the previous Section.

As discussed in Section 2, each transmit frame constitutes a UWB pulse,  $s(t)$ , sampled at  $1/T_s$ . We define frame energy,  $E_p$  as

$$E_p = \sum_{i=0}^{N_s-1} s^2(n, i). \quad (11)$$

We assume all the frames in the transmission are of same pulse shape,  $s(t)$ , and energy,  $E_p$ . As discussed in (2), the received signal under both hypotheses,  $H_1$  and  $H_0$  is corrupted by AWGN noise samples,  $w(n, i)$ . We assume that these noise samples are independent and identically distributed (IID) with  $w(n, i) \sim \mathcal{N}(0, \sigma^2/N_s)$ , where  $\mathcal{N}$ , denotes the normal distribution, such that the total noise energy in the frame is given by

$$\sum_{i=0}^{N_s-1} \mathbf{E}[w^2(n, i)] = \sigma^2. \quad (12)$$

Here,  $\mathbf{E}$ , denotes the expectation operator. We define signal-to-noise ratio, SNR, as

$$\text{SNR} = \frac{E_p}{\sigma^2}. \quad (13)$$

Typical detector structure used in Fig 1 is as shown in Fig. 4. Each detector will construct a test statistic,  $T_k$ , such that

$$T_k = \sum_{n=0}^{N_p^k} \sum_{i=0}^{N_s-1} f_k(r(n, i)), \quad (14)$$

from the received samples and compare it with a threshold to decide on a hypothesis. Depending on the test statistic generation function,  $f_k(\cdot)$ , we have different types of detectors like matched filter, energy detector, amplitude detector, etc,. In this paper, we use MF, ED, and AD detectors, thus we have,  $k \in \{\text{MF, ED, AD}\}$ .  $N_p^k$  denote number of frames used by the detector- $k$ , in the hypothesis testing. The  $r(n, i)$ , denotes the received samples and is equal to  $x(n, i)$  and  $w(n, i)$  during hypotheses  $H_1$  and  $H_0$  respectively.



#### 4.1 Matched Filter

For matched filter, the test statistic in (14) will have

$$f_{\text{MF}}(r(n, i)) = r(n, i)s(n, i). \quad (15)$$

The performance in terms of probability of detection for matched filter,  $P_{\text{D}}^{\text{MF}}$ , as a function of probability of false alarm,  $P_{\text{FA}}^{\text{MF}}$ , and SNR is derived in Appendix-1 and it is given by

$$P_{\text{D}}^{\text{MF}} = \mathbf{Q} \left( \mathbf{Q}^{-1}(P_{\text{FA}}^{\text{MF}}) - \sqrt{N_{\text{s}} N_{\text{p}}^{\text{MF}} \text{SNR}} \right), \quad (16)$$

where  $\mathbf{Q}$  is the tail probability of the standard normal distribution.

#### 4.2 Energy Detector

In energy detector, the test statistic in (14) will have

$$f_{\text{ED}}(r(n, i)) = r^2(n, i). \quad (17)$$

The performance in terms of probability of detection for energy detector,  $P_{\text{D}}^{\text{ED}}$ , as a function of probability of false alarm,  $P_{\text{FA}}^{\text{ED}}$ , and SNR is derived in Appendix-2 and it is given by

$$P_{\text{D}}^{\text{ED}} = \mathbf{Q}_{\chi^2_{\nu}(\lambda)}^{-1} \left( \sqrt{2N_{\text{p}}^{\text{ED}} N_{\text{s}}} \mathbf{Q}^{-1}(P_{\text{FA}}^{\text{ED}}) + N_{\text{p}}^{\text{ED}} N_{\text{s}} \right). \quad (18)$$

Where  $\mathbf{Q}_{\chi^2_{\nu}(\lambda)}$  is the tail probability of the non-central chi-square distribution with  $\nu = N_{\text{p}}^{\text{ED}} N_{\text{s}}$ , degrees of freedom, and centrality parameter,  $\lambda = N_{\text{p}}^{\text{ED}} N_{\text{s}} \text{SNR}$ .

#### 4.3 Amplitude Detector

In the amplitude detector, the test statistic in (14) will have

$$f_{\text{AD}}(r(n, i)) = |r(n, i)|. \quad (19)$$

The performance in terms of probability of detection for amplitude detector,  $P_{\text{D}}^{\text{AD}}$ , as a function of probability of false alarm,  $P_{\text{FA}}^{\text{AD}}$ , and SNR is derived in Appendix-3 and it is given by

$$\begin{aligned} P_{\text{D}}^{\text{AD}} = & \mathbf{Q} \left( \mathbf{Q}^{-1} \left( \frac{P_{\text{FA}}^{\text{AD}}}{2} \right) - \alpha \sqrt{N_{\text{p}}^{\text{AD}} E_{\text{p}} \text{SNR}} \right) \\ & + \mathbf{Q} \left( \mathbf{Q}^{-1} \left( \frac{P_{\text{FA}}^{\text{AD}}}{2} \right) + \alpha \sqrt{N_{\text{p}}^{\text{AD}} E_{\text{p}} \text{SNR}} \right) \end{aligned} \quad (20)$$

where  $\alpha$  is defined as in (21).

$$\sum_{i=0}^{N_{\text{s}}-1} s(i) = \alpha E_{\text{p}}, \quad (21)$$

As shown by (21) and (20), the performance of the amplitude detector depends on the shape of the UWB pulse used. We have considered a normalized second order Gaussian pulse as described in [5, 6, 42]. This is given by

$$s(t) = -4\pi e^{\frac{-2\pi t^2}{\tau^2}} \left( \frac{-\tau^2 + 4\pi t^2}{\tau^4} \right). \quad (22)$$

Here  $\tau$  can be used to control the impulse spread. Energy normalized pulse,  $E_p = 1$ , with  $\tau = 3.33$  ns, sampled at 5 GHz, will result in  $\alpha = 4.49$ . Thus, for this pulse shape the performance of the amplitude detector is given by

$$\begin{aligned} P_D^{AD} = & \mathbf{Q} \left( \mathbf{Q}^{-1} \left( \frac{P_{FA}^{AD}}{2} \right) - 4.49 \sqrt{N_p^{AD} E_p \text{SNR}} \right) \\ & + \mathbf{Q} \left( \mathbf{Q}^{-1} \left( \frac{P_{FA}^{AD}}{2} \right) + 4.49 \sqrt{N_p^{AD} E_p \text{SNR}} \right) \end{aligned} \quad (23)$$

From (16), (18), and (23) the performance of matched filter, energy detector and amplitude detector depends on environment (SNR) and on the system configuration or tuning variables like number of frames considered in the hypothesis testing,  $N_p$  and probability of false alarm,  $P_{FA}$ . In the matched filter and energy detector, the performance is agnostic to the system specifications like pulse shape, which are fixed for a given hardware. However, in the amplitude detector, detection performance depends on the shape of the pulse as shown in (20) and (21). For the parameters from the Table 2, the probability of detection,  $P_D$ , verses SNR using the analytical expression (16), (18), and (23) is as shown in the blue color plots of Fig. 5.

#### 4.4 Simulation Study

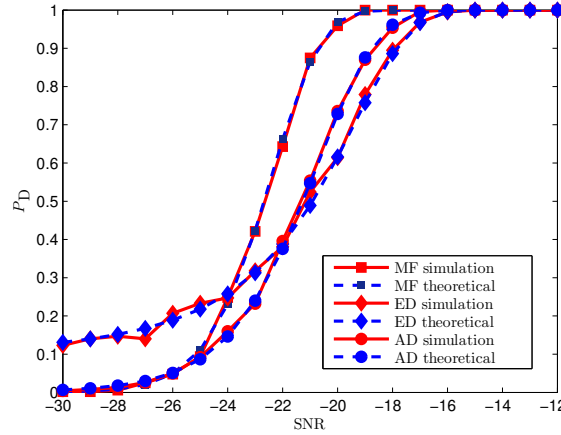
In deriving the energy detector performance equation (18) in Appendix-2, we assumed that a sufficiently large number of pulses are considered. Similarly, for amplitude detector performance equation (23) in Appendix-3, we assumed a particular UWB pulse shape. In this section, we will simulate the detectors and demonstrate the validity of the approximations, for a practical UWB signal setup. We use a signal model in which each frame is of 10 ns duration, having one normalized second order Gaussian pulse as defined in (22) with  $\tau = 3.33$  ns, sampled at 5 GHz. We consider number of frames,  $N_p$ , and the false alarm rate,  $P_{FA}$ , from Table 2 for different detector types. The received samples are corrupted by AWGN noise with variance  $1/\text{SNR}$  (since pulses are normalized, that is  $E_p = 1$ ). Monte-Carlo simulations are done using 1000 independent realizations. The detector performance in simulations shown in red, matches the analytical expressions in (16), (18), and (23), shown in blue in Fig. 5. This validates the derived performance expressions for a practical UWB signal configuration.

### 5 Performance Evaluation of Fusion Methods

When the same radio is used for multiple applications, detectors in them are tuned with different parameter values for  $P_{FA}$ ,  $N_p$ , etc. For example, if the application needs a faster response, then the  $N_p$  used will be small; similarly if the application

**Table 2** Configuration of parameters for different detectors used in the fusion.

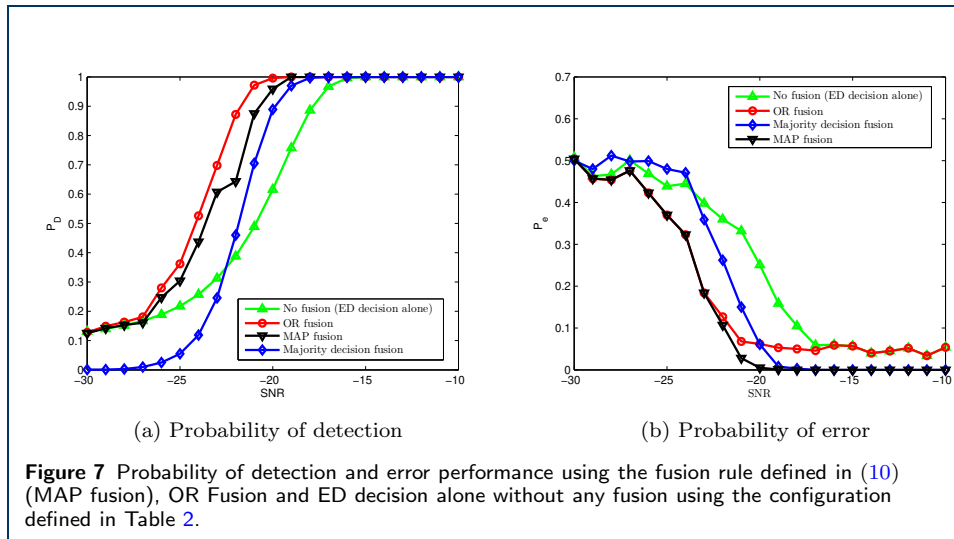
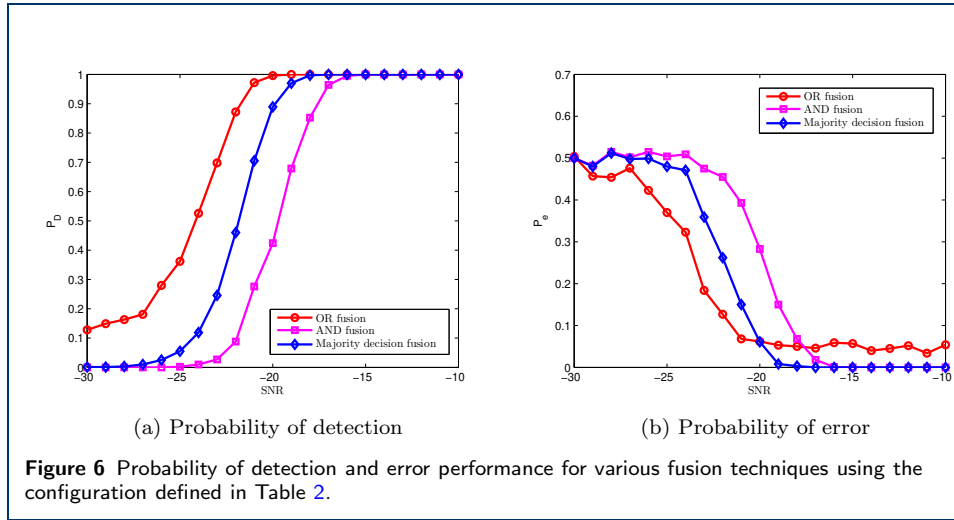
Detector Type	$P_{FA}$	$N_p$
Matched Filter	$10^{-4}$	100
Energy Detector	$10^{-1}$	1000
Amplitude Detector	$10^{-4}$	100

**Figure 5** The performance of different detectors in theory and simulation are shown. A normalized second order Gaussian pulse of width 10 ns sampled at 5 GHz, is used in the simulation. Thousand random realizations are used in building the probability of detection statistics, with parameters from Table 2. The theoretical expressions match the simulation result for all the detectors.

needs robust detection, then it may require a larger  $N_p$ . In general, the parameters  $N_p$ ,  $P_{FA}$  are tuned based on the applications. As a result of this, different detectors are optimal at different SNR regions. For example, consider operating parameters such as probability of false alarm,  $P_{FA}$ , number of frames,  $N_p$ , is as shown in Table 2. Evaluating equations (16), (18) and (20) with false alarm  $P_{FA}$  and number of pulses,  $N_p$  as defined in the Table 2, the probability of detection for different detectors is as shown in blue plots of Fig. 5. We will consider three different types of detectors discussed earlier, i.e., matched filter, energy detector and amplitude detector. With this set of detectors, we have  $L = 3$ , and for “AND”, “OR” and “majority decision”, we should have  $k = 3$ ,  $k = 1$  and  $k > 2$  respectively for  $k$  out of  $L$  fusion rule discussed in Section 3.

We performed Monte-Carlo simulations with similar signal configurations described in Section 4.4. We generated 1000 random signals corresponding to hypotheses,  $H_1$  and  $H_0$  as defined in (1). The probability of correct detection of hypothesis,  $H_1$ , when  $H_1$  was indeed signaled,  $P_D$ , and the probability of mis-classification of hypotheses,  $P_e$ , was evaluated using the fusion rules discussed in Section 3. The false alarm,  $P_{FA}$ , and number of frames employed,  $N_p$ , for each detector type is taken from Table 2. Results for fused probability of detection,  $P_D$ , and probability of error,  $P_e$ , are as shown in Fig. 6a and Fig. 6b respectively. Notice that for a fixed SNR, the probability of detection is high for the “OR” fusion, however, the probability of error is also high for the “OR” fusion. This indicates higher probability of false alarm and probability of miss.

The performance is also evaluated using the MAP fusion rule (10), for a detector set, (MF, ED, AD), yielding decision vector,  $\mathbf{d}$  (refer to Fig. 1), with the configu-



ration taken from Table 2. The probability of detection and probability of error are as shown in Fig. 7a and Fig. 7b, respectively. Notice that the MAP fusion method (defined by (10)) is close to “OR” fusion in detection performance, with superior probability of error performance as shown in Fig. 7b. Comparing the performance of energy detector alone with the MAP fusion rule for multiple detectors in Fig. 7a and Fig. 7b, indicates that a gain of 4 dB in terms of signal to noise ratio (SNR) can be achieved for probability of detection greater than 95% with low probability of error ( $< 5\%$ ).

## 6 Conclusion

In this paper, we analyzed the UWB detection performance of matched filter, energy detector and amplitude detector. We derived the analytical expression for probability of detection,  $P_D$ , for each of the detectors as a function of parameters defined in Table 1. These are shown in (16), (18) and (20). We verified these expressions in simulations, this is shown in Fig. 5. We analyzed the performance in terms of detection probability and probability of error for different fusion methods like “AND”,

“OR” and “majority decision”. This is shown in Fig. 6a and Fig. 6b. Using Bayes rule, we derived an optimal fusion rule (10) for UWB detection, which is optimal in probability of error sense and compared its performance. This is shown in Fig. 7a and Fig. 7b.

Results indicate that by making a suitable choice of fusion rule, a trade off between detection and false alarm can be achieved. For example, Fig. 6a, shows that OR fusion is more biased toward detection, however, it also results in higher errors (due to false alarms, refer to Fig. 6b). If the error performance is critical for the UWB application, then MAP fusion formulation gives superior performance in terms of errors as shown in Fig. 7b. In general, if there are multiple detectors available in the UWB transceiver platform, then decision information from these detectors can be concurrently utilized and intelligently fused based on the application criteria to make a more informed decision on the hypothesis.

## Appendix-1

In this Section, we will derive the analytical expression for probability of detection,  $P_D^{MF}$ , for matched filter. We use  $N_p^{MF}$  received frames in each hypothesis test cycle, having a UWB pulse of energy  $E_p$ , as defined in (11) for  $H_1$  hypothesis and having only noise during the  $H_0$  hypothesis. Due to the AWGN channel the received samples at the receiver have noise which is distributed as,  $w(n, i) \sim \mathcal{N}(0, \sigma^2/N_s)$ , as discussed in Section 4. The total noise energy in the received frame is  $\sigma^2$  as shown in (12). The ratio of frame energy,  $E_p$ , and the noise energy in the received frame,  $\sigma^2$ , is defined as SNR as shown in (13).

In a matched filter, the test statistic,  $T_{MF}$ , is compared against a threshold  $\gamma_{MF}$  (refer to Fig. 4). Thus, the hypotheses test can be formulated as

$$T_{MF} \underset{H_0}{\overset{H_1}{\geq}} \gamma_{MF}, \quad (24)$$

where  $T_{MF}$  is given by

$$T_{MF} = \sum_{n=0}^{N_p^{MF}-1} \sum_{i=0}^{N_s-1} r(n, i)s(n, i). \quad (25)$$

The  $r(n, i)$  and  $s(n, i)$  are defined in Section 4 and 2 respectively. Since,  $r(n, i) = s(n, i) + w(n, i)$  and  $r(n, i) = w(n, i)$  under  $H_1$  and  $H_0$  hypothesis respectively, we can write

$$T_{MF} = \begin{cases} \sum_{n=0}^{N_p^{MF}-1} \sum_{i=0}^{N_s-1} s^2(n, i) + w(n, i)s(n, i) & \text{under } H_1 \\ \sum_{n=0}^{N_p^{MF}-1} \sum_{i=0}^{N_s-1} w(n, i)s(n, i) & \text{under } H_0 \end{cases} \quad (26)$$

Since each transmit frame carry same energy,  $E_p$ , we can write  $\sum_{n=0}^{N_p^{MF}-1} \sum_{i=0}^{N_s-1} s^2(n, i) = N_p^{MF} E_p$ . Thus, the matched filter test statistic under hypothesis  $H_1$ ,

$$T_{MF}^{H_1} = N_p^{MF} E_p + \sum_{n=0}^{N_p^{MF}-1} \sum_{i=0}^{N_s-1} w(n, i) s(n, i). \quad (27)$$

The  $T_{MF}^{H_1}$  is a Gaussian random variable with mean

$$\mathbf{E}[T_{MF}^{H_1}] = N_p^{MF} E_p, \quad (28)$$

and variance

$$\mathbf{Var}[T_{MF}^{H_1}] = \mathbf{Var}[N_p^{MF} E_p] + \sum_{n=0}^{N_p^{MF}-1} \sum_{i=0}^{N_s-1} \mathbf{Var}[s(n, i) w(n, i)], \quad (29)$$

$$= \sum_{n=0}^{N_p^{MF}-1} \sum_{i=0}^{N_s-1} s^2(n, i) \mathbf{Var}[w(n, i)], \quad (30)$$

$$= \frac{N_p^{MF} \sigma^2 E_p}{N_s}, \quad (31)$$

where  $\mathbf{Var}[\cdot]$  denotes the variance of the random variable. Similarly, test statistic under hypothesis  $H_0$ ,  $T_{MF}^{H_0}$ , is a Gaussian random variable with mean and variance

$$\mathbf{E}[T_{MF}^{H_0}] = \mathbf{E}\left[\sum_{n=0}^{N_p^{MF}-1} \sum_{i=0}^{N_s-1} s(n, i) w(n, i)\right] = 0, \quad (32)$$

$$\mathbf{Var}[T_{MF}^{H_0}] = \mathbf{Var}\left[\sum_{n=0}^{N_p^{MF}-1} \sum_{i=0}^{N_s-1} s(n, i) w(n, i)\right] = \frac{N_p^{MF} \sigma^2 E_p}{N_s}. \quad (33)$$

Combining equations (28) to (33), the PDF of the match filter test statistic can be written as

$$p(T_{MF}) = \begin{cases} \mathcal{N}\left(N_p^{MF} E_p, \frac{N_p^{MF} \sigma^2 E_p}{N_s}\right) & \text{under } H_1 \\ \mathcal{N}\left(0, \frac{N_p^{MF} \sigma^2 E_p}{N_s}\right) & \text{under } H_0 \end{cases} \quad (34)$$

where  $p(\cdot)$ , denote the PDF. Thus, for a fixed threshold  $\gamma_{MF}$ , we can show that the match filter detector's probability of false alarm,  $P_{FA}^{MF}$  and probability of detection,  $P_D^{MF}$  is given by

$$P_{FA}^{MF} = \Pr(T_{MF} > \gamma_{MF}; H_0) = \mathbf{Q}\left(\frac{\gamma_{MF}}{\sqrt{\frac{N_p^{MF} \sigma^2 E_p}{N_s}}}\right), \quad (35)$$

$$P_D^{MF} = \Pr(T_{MF} > \gamma_{MF}; H_1) = \mathbf{Q}\left(\frac{\gamma_{MF} - N_p^{MF} E_p}{\sqrt{\frac{N_p^{MF} \sigma^2 E_p}{N_s}}}\right), \quad (36)$$

where  $\mathbf{Q}$  is the tail probability of the Gaussian distribution. By solving for  $\gamma_{\text{MF}}$  in (35) for a fixed false alarm and substituting it in (36), we get the analytical form for the probability of detection. It is given by

$$P_{\text{D}}^{\text{MF}} = \mathbf{Q} \left( \mathbf{Q}^{-1}(P_{\text{FA}}) - \sqrt{N_{\text{s}} N_{\text{p}}^{\text{MF}} \text{SNR}} \right), \quad (37)$$

where SNR is as defined in (13).

## Appendix-2

In this Section, we will derive the analytical expression for the probability of detection,  $P_{\text{D}}$ , for the energy detector. We proceed with the same definitions for  $E_{\text{p}}$ , SNR, and  $\sigma^2$  as in the Appendix-1.

In the energy detector, the test statistic,  $T_{\text{ED}}$ , is compared against a threshold,  $\gamma_{\text{ED}}$  (refer to Fig. 4). Thus, the hypothesis test can be formulated as

$$T_{\text{ED}} \underset{H_0}{\overset{H_1}{\geq}} \gamma_{\text{ED}}, \quad (38)$$

where  $T_{\text{ED}}$  is given by

$$T_{\text{ED}} = \sum_{n=0}^{N_{\text{p}}^{\text{ED}}-1} \sum_{i=0}^{N_{\text{s}}-1} r^2(n, i). \quad (39)$$

The  $r(n, i)$ , is defined in Section 4. Since,  $r(n, i) = s(n, i) + w(n, i)$  and  $r(n, i) = w(n, i)$  under  $H_1$  and  $H_0$  hypothesis respectively, we can write

$$T_{\text{ED}} = \begin{cases} \sum_{n=0}^{N_{\text{p}}^{\text{ED}}-1} \sum_{i=0}^{N_{\text{s}}-1} (s(n, i) + w(n, i))^2 & \text{under } H_1 \\ \sum_{n=0}^{N_{\text{p}}^{\text{ED}}-1} \sum_{i=0}^{N_{\text{s}}-1} w^2(n, i) & \text{under } H_0 \end{cases} \quad (40)$$

If we define the energy detector test statistic under hypothesis  $H_0$  as  $T_{\text{ED}}^{\text{H}_0}$ , then

$$T_{\text{ED}}^{\text{H}_0} = \sum_{n=0}^{N_{\text{p}}^{\text{ED}}-1} \sum_{i=0}^{N_{\text{s}}-1} w^2(n, i). \quad (41)$$

We can modify the random variable,  $T_{\text{ED}}^{\text{H}_0}$  to  $(T_{\text{ED}}^{\text{H}_0} N_{\text{s}})/\sigma^2$ , such that

$$\frac{T_{\text{ED}}^{\text{H}_0} N_{\text{s}}}{\sigma^2} = \sum_{n=0}^{N_{\text{p}}^{\text{ED}}-1} \sum_{i=0}^{N_{\text{s}}-1} l^2(n, i), \quad (42)$$

where  $l(n, i)$ , is an IID with  $\mathcal{N}(0, 1)$ . Thus, the PDF of  $(T_{\text{ED}}^{\text{H}_0} N_{\text{s}})/\sigma^2$  is given by,

$$p \left( \frac{T_{\text{ED}}^{\text{H}_0} N_{\text{s}}}{\sigma^2} \right) \sim \chi_{N_{\text{p}}^{\text{ED}} N_{\text{s}}}^2(0), \quad (43)$$

where  $\mathcal{X}^2$ , denotes the chi-square distribution with degree,  $\nu = N_p^{\text{ED}} N_s$ , and centrality parameter,  $\lambda = 0$ . In (43), the additive nature of chi-square distribution is utilized.

Similarly, the energy detector test statistic under hypothesis  $H_1$ ,  $T_{\text{ED}}^{\text{H}_1}$ , is given by

$$T_{\text{ED}}^{\text{H}_1} = \sum_{n=0}^{N_p^{\text{ED}}-1} \sum_{i=0}^{N_s-1} r^2(n, i). \quad (44)$$

Since,  $r(n, i) = s(n, i) + w(n, i)$ , under  $H_1$ , the received samples under hypothesis,  $H_1$ , will have the distribution,  $r(n, i) \sim \mathcal{N}(s(n, i), \sigma^2/N_s)$ .

If  $X_1, \dots, X_k$ , are  $k$  Gaussian random variables, with mean and variance,  $\mu_i$  and  $\sigma_i^2$  respectively, for  $i \in [1, \dots, k]$ , then the random variable  $\sum_{i=1}^k (x_i/\sigma_i)^2$ , is a chi-square random variable with degree of freedom,  $k$ , and centrality parameter,  $\lambda$ , such that

$$\lambda = \sum_{i=1}^k \left( \frac{\mu_i}{\sigma_i} \right)^2. \quad (45)$$

Therefore from (44), we can write PDF of  $T_{\text{ED}}^{\text{H}_1}$ , as

$$p\left(\frac{N_s T_{\text{ED}}^{\text{H}_1}}{\sigma^2}\right) \sim \sum_{n=0}^{N_p^{\text{ED}}-1} \mathcal{X}_{N_s}^2(\lambda), \quad (46)$$

$$\sim \sum_{n=0}^{N_p^{\text{ED}}-1} \mathcal{X}^2\left(\sum_{i=0}^{N_s-1} \frac{N_s s^2(n, i)}{\sigma^2}\right), \quad (47)$$

Since all frames are of same energy,  $E_p$ , we can write

$$p\left(\frac{N_s T_{\text{ED}}^{\text{H}_1}}{\sigma^2}\right) \sim \sum_{n=0}^{N_p^{\text{ED}}-1} \mathcal{X}_{N_s}^2(N_s \text{SNR}), \quad (48)$$

$$\sim \mathcal{X}_{N_p^{\text{ED}} N_s}^2(N_p^{\text{ED}} N_s \text{SNR}), \quad (49)$$

where in (49), additive nature of the non-central chi-square distribution is exploited. Equations (49) and (43) can be compactly written as

$$p\left(\frac{N_s T_{\text{ED}}}{\sigma^2}\right) = \begin{cases} \mathcal{X}_{N_s N_p^{\text{ED}}}^2(N_p^{\text{ED}} N_s \text{SNR}) & \text{under } H_1 \\ \mathcal{X}_{N_s N_p^{\text{ED}}}^2(0) & \text{under } H_0 \end{cases} \quad (50)$$

If we define,  $N_L = N_p^{\text{ED}} N_s$ , using (42), the PDF of energy detector under  $H_0$ ,  $T_{\text{ED}}^{\text{H}_0}$  can be approximated using central limit theorem (CLT) as

$$p\left(\frac{N_s T_{\text{ED}}^{\text{H}_0}}{\sigma^2}\right) \stackrel{a}{\sim} \mathcal{N}(N_L \mu, N_L \sigma_l^2). \quad (51)$$



Where  $\mu_l$  and  $\sigma_l^2$  are mean and variance of  $l^2(n, i)$ , Since,  $l(n, i)$  is a standard normal with  $\mathcal{N}(0, 1)$ , we can write

$$\mu_l = \mathbf{E}[l^2(n, i)] = 1, \quad (52)$$

$$\sigma_l^2 = \mathbf{E}[l^4(n, i)] - (\mathbf{E}[l^2(n, i)])^2 = 2. \quad (53)$$

Therefore, (51), can be written as

$$p\left(\frac{N_s T_{\text{ED}}^{\text{H}_0}}{\sigma^2}\right) \stackrel{a}{\sim} \mathcal{N}(N_L, 2N_L). \quad (54)$$

Since,  $N_L = N_{\text{p}}^{\text{ED}} N_s$ , we can write

$$p\left(\frac{N_s T_{\text{ED}}^{\text{H}_0}}{\sigma^2}\right) \stackrel{a}{\sim} \mathcal{N}(N_{\text{p}}^{\text{ED}} N_s, 2N_{\text{p}}^{\text{ED}} N_s). \quad (55)$$

From (55), for a fixed false alarm rate of the energy detector,  $P_{\text{FA}}^{\text{ED}}$ , we can compute the threshold,  $\gamma_{\text{ED}}$ , as

$$P_{\text{FA}}^{\text{ED}} = \Pr(T_{\text{ED}}^{\text{H}_0} > \gamma_{\text{ED}}), \quad (56)$$

$$\gamma_{\text{ED}} = \frac{\sigma^2}{N_s} \left[ \sqrt{2N_{\text{p}}^{\text{ED}} N_s} \mathbf{Q}^{-1}(P_{\text{FA}}^{\text{ED}}) + N_{\text{p}}^{\text{ED}} N_s \right]. \quad (57)$$

Using this threshold and from (49), the probability of detection for energy detector,  $P_{\text{D}}^{\text{ED}}$ , is given by

$$P_{\text{D}}^{\text{ED}} = \Pr(T_{\text{ED}}^{\text{H}_1} > \gamma_{\text{ED}}) \quad (58)$$

$$= \mathbf{Q}_{\mathcal{X}_{\nu}^2(\lambda)}^{-1} \left( \sqrt{2N_{\text{p}}^{\text{ED}} N_s} \mathbf{Q}^{-1}(P_{\text{FA}}^{\text{ED}}) + N_{\text{p}}^{\text{ED}} N_s \right) \quad (59)$$

Where  $\mathbf{Q}_{\mathcal{X}_{\nu}^2(\lambda)}$  is the tail probability of the non-central chi-square distribution with degrees of freedom,  $\nu = N_{\text{p}}^{\text{ED}} N_s$ , and centrality parameter,  $\lambda = N_{\text{p}}^{\text{ED}} N_s \text{SNR}$ . The SNR is defined as in (13).

### Appendix-3

In this Section, we will derive the analytical expression for the probability of detection for amplitude detector,  $P_{\text{D}}^{\text{AD}}$ . We proceed with the same definitions for  $E_{\text{p}}$ , SNR, and  $\sigma^2$  as in the Appendix-1.

In the amplitude detector, the test statistic,  $T_{\text{AD}}$ , is compared against  $\gamma_{\text{AD}}$  (refer to Fig 4). Thus, the hypothesis test can be formulated as

$$T_{\text{AD}} \underset{H_0}{\overset{H_1}{\geq}} \gamma_{\text{AD}}, \quad (60)$$

where  $T_{\text{AD}}$  is given by

$$T_{\text{AD}} = \sum_{n=0}^{N_{\text{p}}^{\text{AD}}-1} \sum_{i=0}^{N_s-1} |r(n, i)|. \quad (61)$$

The  $r(n, i)$  is defined in Section 4. Since  $r(n, i) = s(n, i) + w(n, i)$  and  $r(n, i) = w(n, i)$  under  $H_1$  and  $H_0$  respectively, we can write

$$T_{AD} = \begin{cases} \sum_{n=0}^{N_p^{AD}-1} \sum_{i=0}^{N_s-1} |s(n, i) + w(n, i)| & \text{under } H_1 \\ \sum_{n=0}^{N_p^{AD}-1} \sum_{i=0}^{N_s-1} |w(n, i)| & \text{under } H_0 \end{cases} \quad (62)$$

Since noise samples  $w(n, i) \sim \mathcal{N}(0, \sigma^2/N_s)$ , the  $|w(n, i)|$ , has folded normal distribution [43],

$$|w(n, i)| \sim \begin{cases} 2\mathcal{N}(0, \sigma^2/N_s) & \text{when } w(n, i) > 0, \\ 0 & \text{otherwise} \end{cases} \quad (63)$$

Therefore, the amplitude detector test statistic under  $H_0$ ,  $T_{AD}^{H_0} = \sum_{n=0}^{N_p^{AD}-1} \sum_{i=0}^{N_s-1} |w(n, i)|$ , has a PDF given by

$$p(T_{AD}^{H_0}) = \begin{cases} 2\mathcal{N}(0, N_p^{AD}\sigma^2) & \text{when } T_{AD}^{H_0} > 0, \\ 0 & \text{otherwise} \end{cases} \quad (64)$$

Similarly,  $|r(n, i)|$ , under  $H_1$ , also has a folded normal distribution with PDF

$$|s(n, i) + w(n, i)| \sim \begin{cases} \mathcal{N}(s(n, i), \sigma^2/N_s) + \mathcal{N}(-s(n, i), \sigma^2/N_s) & \text{when } r(n, i) > 0, \\ 0 & \text{otherwise.} \end{cases} \quad (65)$$

We use same shape and energy for all the UWB frames and furthermore, we set

$$\sum_{i=0}^{N_s-1} s(n, i) = \alpha E_p, \quad (66)$$

and thus,

$$\sum_{n=0}^{N_p^{AD}-1} \sum_{i=0}^{N_s-1} s(n, i) = \alpha N_p^{AD} E_p. \quad (67)$$

Therefore, the amplitude detector test statistic under  $H_1$ ,  $T_{AD}^{H_1} = \sum_{n=0}^{N_p^{AD}-1} \sum_{i=0}^{N_s-1} |s(n, i) + w(n, i)|$ , has PDF

$$p(T_{AD}^{H_1}) = \begin{cases} \mathcal{N}(\alpha N_p^{AD} E_p, N_p^{AD}\sigma^2) + \mathcal{N}(-\alpha N_p^{AD} E_p, N_p^{AD}\sigma^2) & \text{when } T_{AD}^{H_1} > 0, \\ 0 & \text{otherwise.} \end{cases} \quad (68)$$

For a fixed false alarm rate,  $P_{FA}^{AD}$ , the threshold,  $\gamma_{AD}$  can be computed as

$$P_{FA}^{AD} = \Pr(T_{AD}^{H_0} > \gamma_{AD}). \quad (69)$$

From (64), we can write,

$$\gamma_{AD} = \sqrt{N_p^{AD} \sigma^2} \mathbf{Q}^{-1} \left( \frac{P_{FA}^{AD}}{2} \right) \quad (70)$$

The probability of detection for the amplitude detector,  $P_D^{AD} = \Pr(T_{AD}^{H_1} > \gamma_{AD})$ , From (68), we can write

$$P_D^{AD} = \mathbf{Q} \left( \frac{\gamma_{AD} - \alpha N_p^{AD} E_p}{\sqrt{N_p^{AD} \sigma^2}} \right) + \mathbf{Q} \left( \frac{\gamma_{AD} + \alpha N_p^{AD} E_p}{\sqrt{N_p^{AD} \sigma^2}} \right) \quad (71)$$

Substituting, (70) in (71) and simplifying, we can express the  $P_D^{AD}$  as a function of parameters in Table 1 and is given by

$$\begin{aligned} P_D^{AD} = & \mathbf{Q} \left( \mathbf{Q}^{-1} \left( \frac{P_{FA}^{AD}}{2} \right) - \alpha \sqrt{N_p^{AD} E_p \text{SNR}} \right) \\ & + \mathbf{Q} \left( \mathbf{Q}^{-1} \left( \frac{P_{FA}^{AD}}{2} \right) + \alpha \sqrt{N_p^{AD} E_p \text{SNR}} \right) \end{aligned} \quad (72)$$

#### Competing interests

The authors declare that they have no competing interests.

#### References

1. R.A. Scholtz, "Multiple access with time-hopping impulse modulation," in *Military Communications Conference, 1993. MILCOM '93. Conference record. Communications on the Move., IEEE*, 1993, vol. 2, pp. 447–450 vol.2.
2. M.Z. Win and R.A. Scholtz, "Ultra-wide bandwidth time-hopping spread-spectrum impulse radio for wireless multiple-access communications," *Communications, IEEE Transactions on*, vol. 48, no. 4, pp. 679–689, 2000.
3. Jinyun Zhang, P.V. Orlik, Z. Sahinoglu, A.F. Molisch, and P. Kinney, "UWB Systems for Wireless Sensor Networks," *Proceedings of the IEEE*, vol. 97, no. 2, pp. 313–331, 2009.
4. "First report and order, revision of part 15 of the commission's rules regarding ultra-wideband transmission systems," Tech. Rep., FCC, Washington DC, ET Docket 98-153, 2002.
5. V. Yajnanarayana, S. Dwivedi, A. De Angelis, and P. Händel, "Design of impulse radio UWB transmitter for short range communications using PPM signals," in *Electronics, Computing and Communication Technologies (CONECCT), 2013 IEEE International Conference on*, 2013, pp. 1–4.
6. V. Yajnanarayana, S. Dwivedi, and P. Handel, "Design of impulse radio UWB transmitter with improved range performance using PPM signals," in *Electronics, Computing and Communication Technologies (IEEE CONECCT), 2014 IEEE International Conference on*, Jan 2014, pp. 1–5.
7. K. Witrisal, G. Leus, G. Janssen, M. Pausini, F. Troesch, T. Zasowski, and J. Romme, "Noncoherent ultra-wideband systems," *Signal Processing Magazine, IEEE*, vol. 26, no. 4, pp. 48–66, July 2009.
8. K. Witrisal, G. Leus, G. J M Janssen, M. Pausini, F. Troesch, T. Zasowski, and J. Romme, "Noncoherent ultra-wideband systems," *Signal Processing Magazine, IEEE*, vol. 26, no. 4, pp. 48–66, 2009.
9. Pedro Cruz, Hugo Gomes, and Nuno Carvalho, *Advanced Microwave and Millimeter Wave Technologies Semiconductor Devices Circuits and Systems*, InTech, 2010.
10. Lei Zhu, Sheng Sun, and W. Menzel, "Ultra-wideband (UWB) bandpass filters using multiple-mode resonator," *Microwave and Wireless Components Letters, IEEE*, vol. 15, no. 11, pp. 796–798, Nov 2005.
11. Ching-Luh Hsu, Fu-Chieh Hsu, and Jen-Tsai Kuo, "Microstrip bandpass filters for Ultra-Wideband (UWB) wireless communications," in *Microwave Symposium Digest, 2005 IEEE MTT-S International*, June 2005, pp. 4 pp.–.
12. A Saito, H. Harada, and A Nishikata, "Development of band pass filter for ultra wideband (UWB) communication systems," in *Ultra Wideband Systems and Technologies, 2003 IEEE Conference on*, Nov 2003, pp. 76–80.
13. H. Ishida and K. Araki, "A design of tunable UWB filters," in *Ultra Wideband Systems, 2004. Joint with Conference on Ultrawideband Systems and Technologies. Joint UWBST IWUWBS. 2004 International Workshop on*, May 2004, pp. 424–428.

14. J. Lerdworatawee and Won Namgoong, "Low-noise amplifier design for ultrawideband radio," *Circuits and Systems I: Regular Papers, IEEE Transactions on*, vol. 51, no. 6, pp. 1075–1087, June 2004.
15. Qiuzhen Wan, Qingdi Wang, and Zhiwei Zheng, "Design and analysis of a 3.1-10.6 GHz UWB low noise amplifier with forward body bias technique," *{AEU} - International Journal of Electronics and Communications*, no. 0, pp. –, 2014.
16. P.P. Newaskar, R. Blazquez, and A.P. Chandrakasan, "A/D precision requirements for an ultra-wideband radio receiver," in *Signal Processing Systems, 2002. (SIPS '02). IEEE Workshop on*, Oct 2002, pp. 270–275.
17. ID. O'Donnell and R.W. Brodersen, "An ultra-wideband transceiver architecture for low power, low rate, wireless systems," *Vehicular Technology, IEEE Transactions on*, vol. 54, no. 5, pp. 1623–1631, Sept 2005.
18. B. Murmann, "ADC Performance Survey 1997-2014," <http://web.stanford.edu/~murmman/adcsurvey.html>.
19. John Olof Nilsson, Dave Zachariah, Isaac Skog, and Peter Händel, "Cooperative localization by dual foot-mounted inertial sensors and inter-agent ranging," *EURASIP Journal on Advances in Signal Processing* 2013, vol. Dec. 2013, pp. 164–174, 2013.
20. A. De Angelis, S. Dwivedi, and P. Händel, "Characterization of a Flexible UWB Sensor for Indoor Localization," *Instrumentation and Measurement, IEEE Transactions on*, vol. 62, no. 5, pp. 905–913, 2013.
21. V. Yajnanarayana, S. Dwivedi, A. De Angelis, and P. Händel, "Spectral efficient IR-UWB communication design for low complexity transceivers," *EURASIP Journal on Wireless Communications and Networking*, vol. 2014, no. 1, pp. 158, 2014.
22. K.S. Low, K.M. Lye, and P.K.M. Ho, "Method and apparatus for ultra wide-band communication system using multiple detectors," August 2003, US Patent 6,611,223.
23. Tsang-Yi Wang, "Adaptive UWB Pulse Allocation for Distributed Detection in Sensor Networks," *Communications, IEEE Transactions on*, vol. 59, no. 5, pp. 1357–1367, May 2011.
24. M.Z. Win and R.A. Scholtz, "Impulse radio: how it works," *Communications Letters, IEEE*, vol. 2, no. 2, pp. 36–38, feb. 1998.
25. Nan Guo, Robert C Qiu, Shaomin S Mo, and Kazuaki Takahashi, "60-ghz millimeter-wave radio: Principle, technology, and new results," *EURASIP Journal on Wireless Communications and Networking*, vol. 2007, no. 1, pp. 068253, 2007.
26. "IEEE 802.15.3c Millimeter Wave Alternative PHY," Tech. Rep., IEEE 802.15.3c-2009 Std, 2009.
27. E. Torkildson, U. Madhow, and M. Rodwell, "Indoor millimeter wave mimo: Feasibility and performance," *Wireless Communications, IEEE Transactions on*, vol. 10, no. 12, pp. 4150–4160, December 2011.
28. S.L. Cotton, "A Statistical Model for Shadowed Body-Centric Communications Channels: Theory and Validation," *Antennas and Propagation, IEEE Transactions on*, vol. 62, no. 3, pp. 1416–1424, March 2014.
29. A.F. Molisch, "Ultrawideband propagation channels-theory, measurement, and modeling," *Vehicular Technology, IEEE Transactions on*, vol. 54, no. 5, pp. 1528–1545, 2005.
30. "TransferJet Overview Whitepaper," [http://www.transferjet.org/tj/transferjet\\_whitepaper.pdf](http://www.transferjet.org/tj/transferjet_whitepaper.pdf), 2009.
31. "WiMedia Alliance," <http://www.wimedia.org/>.
32. T Kovattana, "Theoretical Analysis of Intrusion Alarm Using Two Complementary Sensors," in *Proc. of Carnahan Conf. Electronic Crime Countermeasures*, 1973, pp. pp.37–52.
33. A Fefjar, "Combining Techniques to Improve Security in Automated Entry Control," in *Proc. of Carnahan Conf. on Crime Countermeasures*, 1978, p. pp.89.
34. S.D Stearns, "Optimum Detection Using Multiple Sensors," in *Proc. of Carnahan Conf. on Security Technology*, 1983.
35. A.M. Aziz, M. Tummala, and R. Cristi, "Optimal data fusion strategies using multiple-sensor detection systems," in *Signals, Systems and Computers, 1997. Conference Record of the Thirty-First Asilomar Conference on*, Nov 1997, vol. 1, pp. 941–945 vol.1.
36. G.L. Turin, "An introduction to matched filters," *Information Theory, IRE Transactions on*, vol. 6, no. 3, pp. 311–329, June 1960.
37. Harry L Van Trees, *Detection, estimation, and modulation theory*, John Wiley & Sons, 2004.
38. Harry Urkowitz, "Energy detection of unknown deterministic signals," *Proceedings of the IEEE*, vol. 55, no. 4, pp. 523–531, April 1967.
39. S.M. Kay, *Fundamentals of Statistical Signal Processing: Detection theory*, Prentice Hall Signal Processing Series. Prentice-Hall PTR, 1998.
40. I. Guvenc and Z. Sahinoglu, "Threshold-based TOA estimation for impulse radio UWB systems," in *Ultra-Wideband, 2005. ICU 2005. 2005 IEEE International Conference on*, Sept 2005, pp. 420–425.
41. I. Guvenc, Z. Sahinoglu, and P.V. Orlik, "TOA estimation for IR-UWB systems with different transceiver types," *Microwave Theory and Techniques, IEEE Transactions on*, vol. 54, no. 4, pp. 1876–1886, June 2006.
42. R. Kohno M. Ghavami, L.B. Michael, *Ultra Wideband Signals and Systems in Communication Engineering*, John Wiley, West Sussex, UK, 2007.
43. F. C. Leone, L. S. Nelson, and R. B. Nottingham, "The folded normal distribution," *Technometrics*, vol. 3, no. 4, pp. 543–550, 1961.